A preliminary computational analysis towards the use of Electrically Heated Mixing Catalyst for innovative SCR after-treatment systems

A preliminary computational analysis towards the use of Electrically Heated Mixing Catalyst for innovative SCR after-treatment systems

A. Nappi, A. Vespertini, A. Della Torre, G. Montenegro and A. Onorati

Dipartimento di Energia, Politecnico di Milano, Milano, Italy.

E-mail: antonello.nappi@polimi.it, andrea.vespertini@polimi.it, augusto.dellatorre@polimi.it, gianluca.montenegro@polimi.it, angelo.onorati@polimi.it

Abstract. This work aims at investigating the possible advantages of substituting the mixer in traditional SCR systems with an Electrically Heated Catalytic structure (EHC). First of all, EHC technology is being widely investigated in literature because it offers a concrete solution for catalyst thermal activation and film formation reduction in engine cold start conditions; however, its adoption as a mixer can also guarantee other important improvements in reducing pollutant emissions. In this work, a low-pressure injection of Ad-Blue impacts an electrically heated structure and a complete analysis of liquid droplets and film evaporation is carried out. A hybrid Eulerian-Lagrangian model has been adopted on a multi-region configuration, accounting for fluid-solid conjugate heat transfer (CHT), which plays a key role in the conversion strategy: it has been demonstrated that the heated structure can be exploited to significantly increase the exhaust gas enthalpy in the cold start, which represents an important improvement for pollutant conversion. Different heating strategies are analysed, with the objective of maximising the spray evaporation and the uniformity of the ammonia distribution downstream of the mixer. The objectives of this work are emphasizing the improvements that an electrically heated mixing catalyst can bring to the traditional SCR configuration, laying the foundation for other following studies.

1. Introduction

In the last decades, the introduction of more stringent regulations for the pollutant emissions of vehicles has spurred the development of more efficient after-treatment technologies [1]. Selective catalytic reduction (SCR) is one of the prominent technologies used for the abatement of NOx: the reduction of NOx in these systems is performed through the use of ammonia, introduced in the exhaust stream as urea water solution (UWS). After the injection, the atomized stream of UWS is heated up by the interaction with the exhaust gases and undergoes a hydrolysis and thermolysis process [2], which converts the urea contained in UWS into gaseous ammonia. The ammonia formed must be fed to the catalyst, making sure that its distribution is as uniform as possible, to achieve the maximum NOx conversion efficiency. As the atomization of the low-pressure injectors used to provide UWS is low, the interaction between the spray and the walls of the SCR system is inevitable. This interaction can lead to localized cooling [3] and the formation of a permanent film, which is the main source of solid deposits. The formation of these deposits

is not only detrimental to the operation of the SCR system (as they can lead to clogging) but also alters the dosing strategy of ammonia, causing a reduction of the conversion efficiency. The startup phase of the engine represents a critical phase for the operation of the SCR system, as the temperatures of the components are well below the deposition temperature, and the fraction of UWS converted into ammonia is low, due to a reduced evaporation rate of the spray. To improve the performance of the system in these conditions, electrically heated catalyst (EHC) structures can be used in the role of both a pre-catalyst and a mixer: the possibility of adopting it as a mixer in an SCR after-treatment system has already been investigated in [4]. In particular, in this paper, a preliminary analysis is performed by considering a simplified structure representing a single row of struts of an EHC, and showing how different heating strategies can improve the conversion of UWS into ammonia in the cold start. The analysis has been carried out adopting an advanced numerical model, which is able to consider heat/mass transfer between fluid and solid domains transfer, spray-wall interaction (including also the possibility of wall-film formation) and an electrostatic model for the solid region, which is capable to estimate the power delivered by the joule heating effect and also the current flowing in the structure.

2. Governing equations

These simulations are carried out in a multi-region environment and require solving different governing equations for each domain and to couple these regions to describe their reciprocal influence. The finite volume method approach was used in this work together with a Lagrangian description of the spray, described in [5]. In the next sections, a more in-depth description will be given of some of the most important models that were used in these simulations.

2.1. Fluid region

To simulate the fluid flowing inside the square duct, a model already proposed in [5] has been adopted, which includes the conservation equations for the mass, momentum, energy and chemical species: in the Navier-Stokes equations, source terms were added to keep into account for the presence of both the Lagrangian phase and the Eulerian. The turbulence of the fluid flow has been handled with the adoption of $k-\omega SST$ model, which introduces two transport equations for the turbulent kinetic energy k and the specific dissipation rate ω.

2.2. Spray wall interaction

The description of the spray wall interaction is a complex topic, with many parameters influencing the outcome of this. Several models were proposed [6], and in this work, the Kuhnke model [7] was used. In this model, four different impact regimes are distinguished: rebound, thermal breakup, deposition and cold splash. These four different regimes are distinguished by using two parameters:

- the thermal parameter T^*, defined as the ratio between wall temperature and the droplet saturation temperature;
- the kinematic parameter defined in [8]:

$$K = We^{\frac{5}{8}} La^{\frac{1}{8}} \tag{1}$$

where We and La are the Weber and Laplace number, defined respectively as $We = \frac{\rho v^2 l}{\sigma}$ and $La = \frac{\sigma \rho l}{\mu^2}$. In Fig.(1b) the impingement map is represented, highlighting the boundaries between the different impingement regimes. First of all, a unique T^*_{crit} is used to distinguish between the cold wall and hot wall interaction. The value of T^*_{crit} is still debated, and ranges from 1.1 [7] to 1.43-1.47 [9]. This value has fundamental importance as it is also used as the deposition threshold, meaning that under this temperature the formation of a wall film is

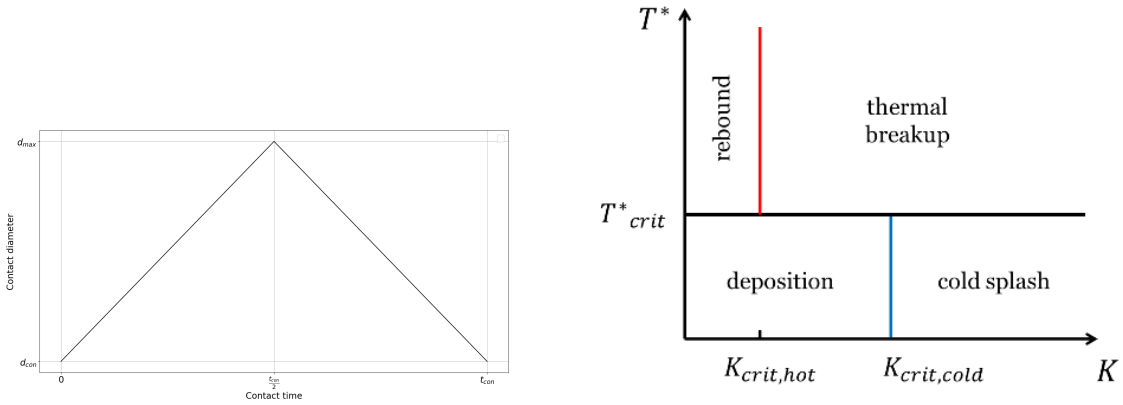

(a) (b)

Figure 1: In Fig.1a contact diameter, as a function of contact time (t_{con}) has been reported. Fig. 1b represents a T^* vs K diagram, with different impact regimes.

allowed, influencing the heat transfer with the wall. For the distinction between destructive and non-destructive interactions, the value of the K_{crit} is not univocal, and two different values are used: $K_{crit,hot}$ to distinguish between rebound and thermal breakup and $K_{crit,cold}$ to separate deposition and cold splash. The evaluation of the We number required to calculate the K parameter is done using the normal component of the velocity since no influence of the impingement angle is found in the literature. For a more extensive description of the model, the read is referred to the articles [3]-[10]. During the interaction between wall and droplets, the heat exchanged is calculated using a semi-infinite body approach, as proposed by [11]:

$$Q = A_{con} \frac{2\sqrt{t_{con}}}{\sqrt{\pi}} \frac{b_w b}{b_w + b} (T_w - T) \quad , \tag{2}$$

where A_{con} is the contact area, t_{con} is the contact time and b_w, b represents the effusivities of the wall and of the droplet, respectively. Both A_{con} and t_{con} depend on the impingement regimes, through the value of K and of the We number. The contact area is considered to have a triangular profile, as shown in Fig(1a). The Wruck formula is unable to take into account the effect of the wall overheating on the heat flux, meaning that a correction is needed to capture the transition between the different temperature regimes. To do so, the heat exchanged calculated from the Wruck formula is used to calculate an equivalent heat transfer coefficient (HTC):

$$HTC_{wruck} = \frac{Q}{A_{con} \Delta T \delta_{time}} \quad , \tag{3}$$

where ΔT and δ_{time} represent the temperature difference between solid and droplet and the time step, respectively. This HTC is then compared with the one obtained from a model equivalent to the one which has been developed for the wall film, which will be introduced later, and reduced if necessary.

2.3. Liquid film modelling

For this case, the multi-species wall film model presented in [5] was used. This model defines a single-layer region where the conservation equation (mass, momentum, energy and species) are solved. Since in this case the film region is defined on the surface of heated struts, correctly

evaluating the heat transfer between the struts and the film is fundamental. To do so, a model was developed, based on the Nukiyama curve, that evaluates the heat flux between the film and the wall as a function of the excess temperature (ΔT_e), defined as the difference between the wall temperature and the saturation temperature of the film (or the droplet, when the model is applied to the spray). For each different evaporation regime different correlations are used to

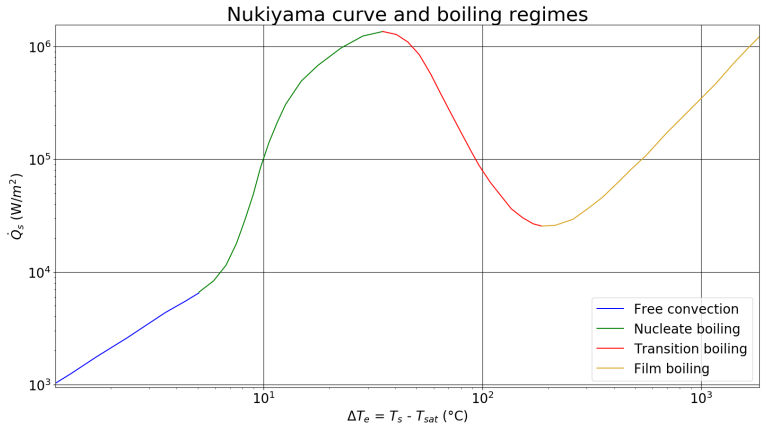

Figure 2: Nukiyama boiling curve for water.

evaluate the heat flux, and in particular:

- in the free convection regime ($\Delta T_e < 5$) the heat flux is calculated as a linear interpolation between the minimum heat flux for nucleate boiling, and the heat flux due to pure conduction;
- in the nucleate boiling regime ($5 < \Delta T_e < 65$), the heat flux is evaluated using a sigmoid interpolator, constructed from data available for water;
- in the transition regime ($65 < \Delta T_e < 170$), the heat flux is evaluated as the linear interpolation between the maximum heat flux at the critical heat flux (CHF) temperature and the value at the Leidenfrost point;
- finally, for temperatures above the Leidenfrost point, the heat flux is fixed to the value at the Leidenfrost point.

The heat flux is then used to evaluate an HTC, which is in turn used to calculate the heat fluxes to the wall and the film.

2.4. Solid modelling: heat transfer and electrostatic equations

In the solid domain, the energy equation is given by the equation of heat conduction (Eq.4):

$$Q(r,t) = -k\nabla T(r,t) \quad , \tag{4}$$

where the key parameter is the thermal conductivity k which is an intrinsic property of the material considered.

As already suggested in the first chapter, a possible solution for increasing fluid enthalpy, reducing cold start problems and avoiding film formation is represented by the electrical heating of the solid structures.

First of all, the evolution of the voltage scalar field V inside the solid domain is granted by the

solution of the parabolic differential equation 5, where the velocity of the spatial diffusion is linked to the electrical conductivity σ.

$$\frac{\partial V}{\partial t} = \sigma \nabla^2 V \quad , \tag{5}$$

$$\vec{J} = -\sigma \nabla V \quad , \tag{6}$$

$$\frac{dQ}{d\tau} = -\vec{J} \cdot \nabla V \quad , \tag{7}$$

Furthermore, the current density $\vec{J}$ is defined within the solid domain (eq. 6), with the convention of positive values of current density with negative velocity gradient: this quantity is then used to estimate the power generated per unit of volume (eq. 7), which is added directly in the energy conservation equation as a heat source term.
Finally, the solid domain is linked with the reacting one, hence to the fluid, thanks to a dedicated boundary condition which keeps into account the boundary faces distance to each cell center $L_{i,j}$, the conductivity of the region $\lambda_{i,j}$ and the temperature of the cell center $T_{i,j}$: this boundary condition imposes a temperature T_w on the boundary patch given by the two contributions:

$$T_w = T_i - \frac{\lambda_j L_i}{\lambda_i L_i + \lambda_j L_j} (T_i - T_j) \quad , T_w = T_j + \frac{\lambda_i L_j}{\lambda_i L_i + \lambda_j L_j} (T_i - T_j) \quad , \tag{8}$$

3. EHC simulation

In this section, the developed test case will be presented, starting from the geometry chosen and then presenting the mesh generation process, the case setup and the results obtained.

3.1. Geometry

To represent a generic strut of an electrically heated catalyst, four cylinders with a 4 mm diameter were placed in a rhomboidal shape. The pitch was taken to be the same in both directions ($2cm$). To make sure that all of the four struts were heated uniformly, two large plates were also added at the top and bottom of the struts, to make sure that the voltage drop across all struts was the same. The cylinders and the plates are both supposed to be made of Tungsten. The fluid domain is defined by a tunnel with a square cross-section ($6 \cdot 10^{-4} m^2$) and a length of $0.2m$.

3.2. Mesh

Region	Cell number	Max non-orthogonality	min cell dimension
Fluid	1582528	65.4	$9.5 \cdot 10^{-5}$ mm
Strut	40128	65.4	$9.5 \cdot 10^{-5}$ mm
Plates	834336	25.2	$3 \cdot 10^{-4}$ mm
Film	21120	0.86	$9.5 \cdot 10^{-5}$ mm

Table 1: Mesh properties for each domain.

The mesh was generated by starting from a hexahedral background mesh which was then conformed to the geometry, leading to a hex-dominant mesh: this has been then split into the different regions needed for this simulation. Then, to account for the presence of the film, three

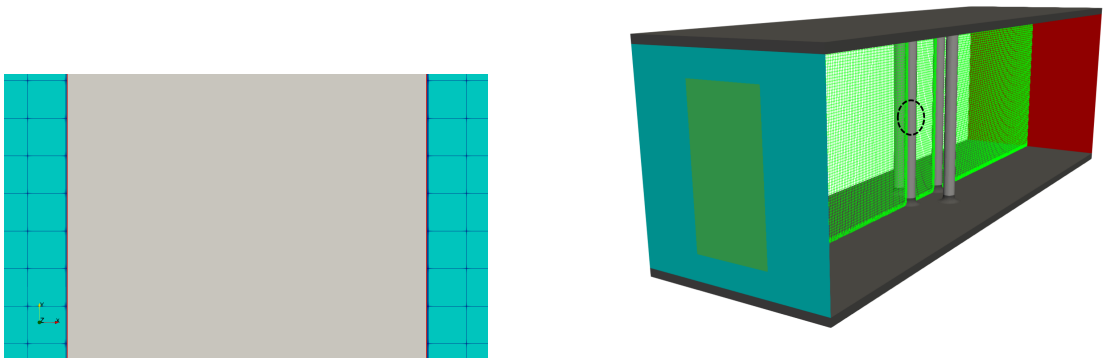

(a) (b)

Figure 3: In Fig. 3a the details of the mesh generation process are shown for the first cylinder circled in Fig. 3b: in particular, the presence of the thin layer characterizing the film region is highlighted in red. In Fig. 3b, a representation of the computational mesh is reported, showing the main computational boundaries and a slice of the fluid internal mesh.

thin layers have been extruded around the cylinders and the nearest to the fluid-solid boundary was considered to be the liquid film domain (Fig. 3a). In Fig. (3b), the final mesh is shown with the struts in light grey, the plate in dark grey and the outlet patch in red. The inlet patch (light blue) has an inner section (green) which will be used for the injection of the liquid spray. Some data on the meshes for each region are listed in Table (1).

3.3. Setup

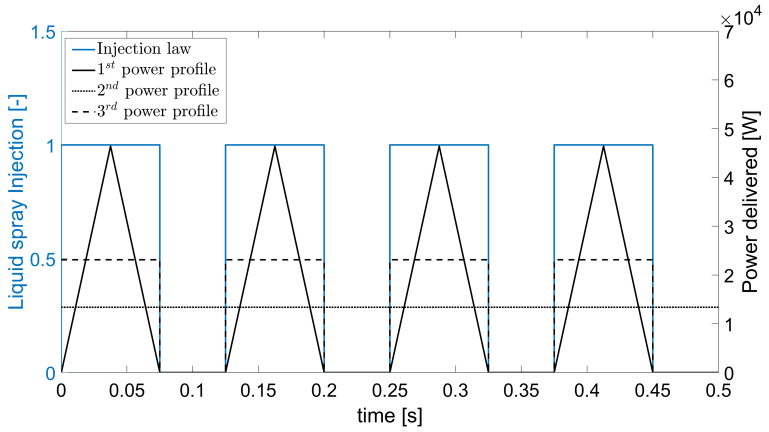

Figure 4: Liquid spray flow profile and the three different profiles for power delivered by the cylindrical struts.

As already mentioned in Section 3.2, a rectangular patch was derived from the inlet and was used to perform a uniform injection of liquid droplets whose flow profile has been reported in Figure 4: an 8Hz injection of Adblue was considered during the whole simulating time (0.5s), having a total injected mass of 1g, an injection velocity of 28m/s and a Gaussian distribution for droplets diameter centred at $10^{-4}m$, as this value is representative of the typical droplets in a common low-pressure injector (such as the one adopted in SCR systems). To simulate

Fluid region	
U_{inlet}	$10\frac{m}{s}$
T_{fluid}	$300K$
$T_{fl/film}$	$300K$
Solid region	[Tungsten]
$Voltage$	$[1, 1.8]V$ (Fig. 4)
T_{solid}	$300K$
Liquid film	
T_{film}	$300K$

Table 2: More relevant boundary conditions for fluid, solid and film domains

a cold start condition, values in Table 2 have been used as initial boundary conditions for the simulation. As can be understood in Fig. 4 from the power curves, three voltage profiles (coupled in time with the injection of the spray) have been applied to the top plate of the solid region, while the bottom is set to ground. The first profile is a simple sawtooth, having a voltage peak of $\sim 1.86V$, the second is a constant $V = 1V$ and the third is stepped, with a peak value of $\sim 1.32V$: this choice has been done to have three injection profile with the same amount of energy delivered during the whole injection time, which was set to $\sim 6.5kJ$.

3.4. Results

To evaluate the effectiveness of each heating strategy, two different parameters were evaluated: the mass of water evaporated and the increase in gas temperature. Both quantities were evaluated by calculating the difference between two planes, one 3mm before and one 5.5mm after the struts (along the x axis). The mass of water evaporated is shown in Figure (5). It can

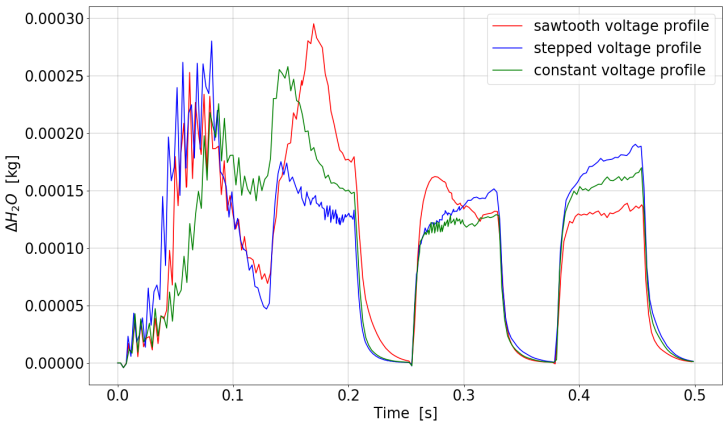

Figure 5: Mass of water evaporated.

be seen how for the first two injections no heating strategy other than the stepped one, manages to completely evaporate the film which forms on the struts as the mass of water never goes to

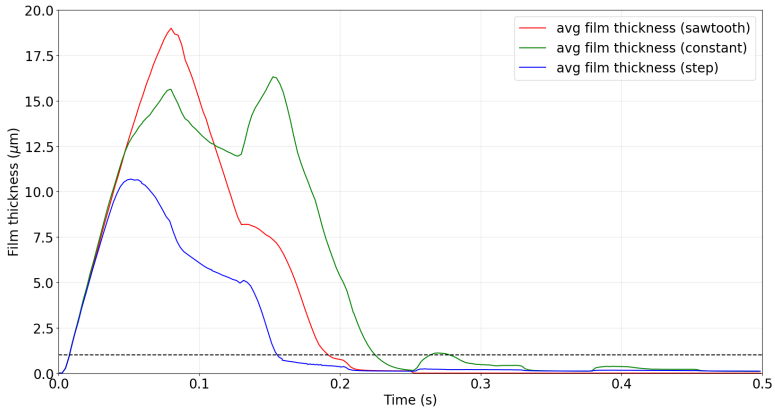

Figure 6: Average film thickness: the dashed line represents the threshold value of film height for the activation of conjugate heat transfer with the film.

zero, as can be seen in Figure (6). In these low strut temperature conditions, the sawtooth and stepped voltage profiles show better performances, with a higher evaporating mass concerning the constant voltage strategy. For the first injection, the mass of water evaporated shows strong fluctuations, as multiple phenomena (film formation and evaporation, stripping from the film, droplet breakup) overlap. In the first inter-injection period (around 0.12 s), it can be noticed as the constant voltage strategy keeps on evaporating the film deposited on the structure. For the second injection only the sawtooth and constant voltage strategy show film deposition and evaporation. This effect can be justified as the sawtooth profile high peak power is less effective than the stepped voltage strategy at heating the strut, leading to the absence of film deposition from the second injection for the stepped case, as can be seen in Figure (6). Still, the effect of the higher peak power can be seen again by looking at the second injection event, where the sawtooth profile shows the highest evaporating mass of all the simulations.

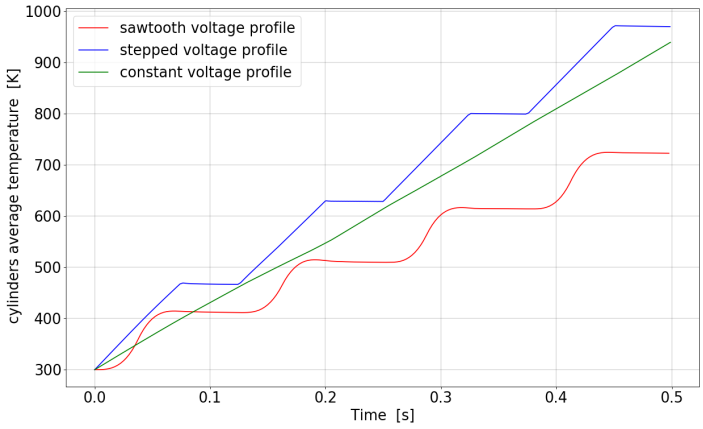

Figure 7: Average strut temperature.

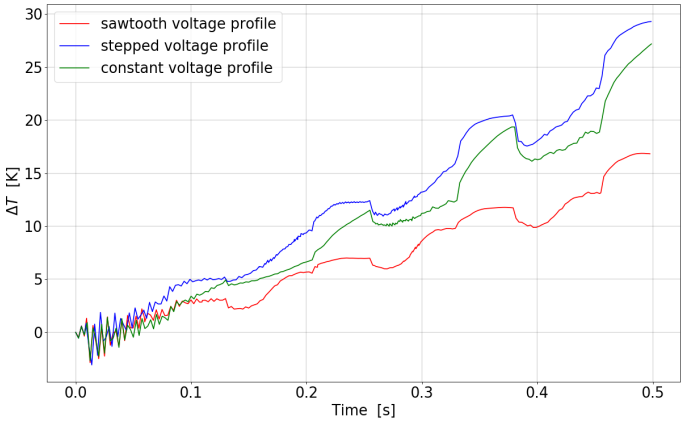

Figure 8: Gas temperature increase across structure.

The third injection event captures a transitional behaviour for spray wall heat exchange, as the increase in strut temperature entails a transition between evaporation regimes. In this case, the sawtooth profile, due to its lower temperature shows higher evaporation at the start of the injection, which reduces as the temperature of the solid increases, showing the transition from nucleate boiling heat transfer to transition boiling (see Figure 7), which is accompanied by a reduction of the HTC between spray and strut. In the fourth injection, as for all the four structures the heat exchange is under film boiling conditions, the structures with the higher temperature show again the higher evaporation, justifying the trend shown in the figure.
Another important use of such heated catalysts is as a heater for the cold air flowing through the exhaust system. This is important as the catalyst itself is then heated by this air, and therefore a higher heating capability is fundamental to ensure that the cold start period for these systems is reduced as much as possible. As it can be seen, for all the heating strategies the increase in temperature obtained is modest, but this is due to the low wetted surface of the simplified structure and will increase going from this test structure to a real system. Comparing the different voltage strategies on this performance shows that the stepped and constant voltage strategies show a superior heating capability (see Fig. 8), as they both manage to heat the solid structure more, thus leading (given that for all four cases the heat transfer coefficient is similar) to a higher heat flux directed toward the gas. It can be noticed that the stepped strategy shows better behaviour for the second injection, as it was the only strategy where no film deposition occurred on the second injection.

4. Conclusions

In this work, a simplified structure meant to represent a single layer of a generic EHC was simulated in conditions typical of the cold start of an internal combustion engine. Different heating strategies were tested, under the iso-energy hypothesis for all strategies: a constant voltage strategy, a stepped voltage strategy and a sawtooth profile strategy. To evaluate the performance of the system, two parameters were chosen: the mass of water evaporated and the temperature increase, both evaluated after the structure. Regarding the first performance, the stepped profile and sawtooth profile have shown good behaviour when starting from low temperatures, as they both can rapidly heat the structure and evaporate any film formed, due to their higher peak power concerning the constant voltage strategy. In particular, the stepped

voltage strategy appears to be the fastest at heating the structure, as the sawtooth profile strategy suffers from a delay in the heating of the structure due to the ramp-up period of the voltage. This can be improved by using a different phasing of the voltage increase concerning the injection, making sure that when the first droplet reaches the structure the power delivered to the EHC is already high enough to quickly evaporate them. Regarding the performance of the structure as a heater, it is apparent that the stepped and constant voltage strategies, in this case, allow more effective heating of the gases, as they achieve higher average strut temperatures, meaning that in the same fluid-dynamic conditions the heat flux toward the gas will be higher. This is important as the initial heating of the CAT can be improved by the heating provided by the structure, reducing the time to the light off of the reactions. Finally, a preliminary assessment of the positive effects of substituting a mixer with an electrically heated catalyst can be summarized as the following points:

- an increase in the fluid enthalpy, which can be improved by increasing the wetted surface;
- an increase in the evaporation of the UWS spray, which leads to a higher formation of ammonia at low gas temperatures.

To have a complete comparison with the existing mixers on the market, the performances of both systems need to be put under scrutiny in the same conditions, considering the same exhaust system geometry, and performing a substitution of a generic mixer with an EHC.

References

[1] T.Johnson. Review of vehicular emissions trends. *Environmental Science- SAE International Journal of engines*, 2015.
[2] M. Koebel and E. O. Strutz. Thermal and hydrolytic decomposition of urea for automotive selective catalytic reduction systems: Thermochemical and practical aspects. 2003.
[3] A. Nappi, G. Montenegro, A. Onorati, A. Della Torre, and D. Eggenschwiler. Modeling the kinetic and thermal interaction of uws droplets impinging on a flat plate at different exhaust gas conditions. *SAE technical papers*, 2021.
[4] A. Vespertini, A. Della Torre, G. Montenegro, A. Onorati, E. Tronconi, and I. Nova. An appraisal of the application of open-cell foams in automotive scr systems. *E3S Web of Conferences 197*, 2020.
[5] A. Nappi, G. Montenegro, A. Onorati, and A. Della Torre. A cht framework for the cfd analysis of the spray-wall thermal interaction in the dosing unit of scr systems for diesel engines. *E3S Web of Conferences*, 2019.
[6] C. Bai and A. D. Gosman. Development of methodology for spray impingement simulation. *SAE Technical Paper*, 1995.
[7] D. Kuhnke. *Spray-wall interaction modelling by dimensionless data analysis*. Aachen:Shaker, 2004.
[8] Chr.Mundo, M.Sommerfeld, and C.Tropea. Droplet-wall collisions: Experimental studies of the deformation and breakup process. 1995.
[9] F. Birkhold, U. Meingast, P. Wassermann, and O. Deutschmann. Analysis of the injection of urea-water-solution for automotive scr denox-systems: Modeling of two-phase flow and spray/wall-interaction. 2006.
[10] Lorenzo Nocivelli. *Cfd modeling and experimental characterization of urea/water solution injection inside SCR systems of diesel engines*. PhD thesis, 01 2017.
[11] N. Wruck and U. Renz. Transientes sieden von tropfen beim wandaufprall. 1995.